European Journal of Pharmaceutical Sciences 190 (2023) 106571

Contents lists available at ScienceDirect

European Journal of Pharmaceutical Sciences

journal homepage: www.elsevier.com/locate/ejps

Liposome-encapsulated zoledronate increases inflammatory macrophage population in TNBC tumours

Nataliia Petruk [a,1], Sofia Sousa [b,1], Martine Croset [c], Lauri Polari [a,d], Hristo Zlatev [b], Katri Selander [e], Jukka Mönkkönen [b], Philippe Clézardin [c], Jorma Määttä [a,f,*]

[a] Institute of Biomedicine, University of Turku, Turku, Finland
[b] School of Pharmacy, University of Eastern Finland, Kuopio, Finland
[c] INSERM, UMR_S1033, University of Lyon, Lyon, France
[d] Faculty of Science and Engineering, Cell Biology, Åbo Akademi University, Turku, Finland
[e] Department of Oncology and Radiation Therapy, Oulu University Hospital, Oulu, Finland
[f] Turku Center for Disease Modeling, University of Turku, Turku, Finland

ARTICLE INFO

Keywords:
Breast cancer
Zoledronate
Tumour-associated macrophages
Inflammation

ABSTRACT

Background: Tumour associated macrophages (TAMs) are important players in breast tumour progression and metastasis. Clinical and preclinical evidence suggests a role for zoledronate (ZOL) in breast cancer metastasis prevention. Further, zoledronate is able to induce inflammatory activation of monocytes and macrophages, which can be favourable in cancer treatments. The inherent bone tropism of zoledronate limits its availability in soft tissues and tumours. In this study we utilised an orthotopic murine breast cancer model to evaluate the possibility to use liposomes (EMP-LIP) to target zoledronate to tumours to modify TAM activation.

Methods: Triple-negative breast cancer 4T1 cells were inoculated in the 4th mammary fat pad of female Balb/c mice. Animals were divided according to the treatment: vehicle, ZOL, EMP-LIP and liposome encapsulated zoledronate (ZOL-LIP). Treatment was done intravenously (with tumour resection) and intraperitoneally (without tumour resection). Tumour growth was followed by bioluminescence *in vivo* imaging (IVIS) and calliper measurements. Tumour-infiltrating macrophages were assessed by immunohistochemical and immunofluorescence staining. Protein and RNA expression levels of inflammatory transcription factors and cytokines were measured by Western Blotting and Taqman RT-qPCR.

Results: Liposome encapsulated zoledronate (ZOL-LIP) treatment suppressed migration of 4T1 cell *in vitro*. Tumour growth and expression of the angiogenic marker CD34 were reduced upon both ZOL and ZOL-LIP treatment *in vivo*. Long-term ZOL-LIP treatment resulted in shift towards M1-type macrophage polarization, increased CD4 T cell infiltration and activation of NF-κB indicating changes in intratumoural inflammation, whereas ZOL treatment showed similar but non-significant trends. Moreover, ZOL-LIP had a lower bisphosphonate accumulation in bone compared to free ZOL.

Conclusion: Results show that the decreased bisphosphonate accumulation in bone promotes the systemic anti-tumour effect of ZOL-LIP by increasing inflammatory response in TNBC tumours via M1-type macrophage activation.

Abbreviations: AppI, triphosphoric acid 1-adenosin-5′-yl ester 3-(3-methylbut-3-enyl) ester); BC, breast cancer; BP, bisphosphonate; BV, bone volume; EMP-LIP, empty liposome; FPPS, farnesyl pyrophosphate synthase; IL, interleukin; IP, intraperitoneal; IPP, isopentenyl pyrophosphate; IV, intravenous; IVIS, *in vivo* imaging system; LIP, liposome; N-BP, nitrogen-containing BP; N.Oc., number of osteoclasts; PEG, polyethylene glycol; TAMs, tumour associated macrophages; TNBC, triple-negative breast cancer; TV, tissue volume; ZOL, zoledronate; ZOL-LIP, liposome-encapsulated ZOL.

* Corresponding author at: Institute of Biomedicine, University of Turku, Turku, Finland.
E-mail address: jmaatta@utu.fi (J. Määttä).

[1] These authors contributed equally to this work.

https://doi.org/10.1016/j.ejps.2023.106571
Received 8 March 2023; Received in revised form 23 August 2023; Accepted 28 August 2023
Available online 29 August 2023

1. Introduction

Nitrogen-containing bisphosphonates (N-BPs) inhibit the mevalonate pathway that leads to intracellular accumulation of isopentenyl pyrophosphate (IPP) and triphosphoric acid 1-adenosin-5′-yl ester 3-(3-methylbut-3-enyl) ester (ApppI). The primary use of N-BPs is to prevent osteoporosis via osteoclast inhibition (Roelofs et al., 2006). However, pre-clinical data have demonstrated anti-cancer effects of N-BPs to induce cancer cell apoptosis after IPP and ApppI accumulation (Mitrofan et al., 2009). Zoledronate, as a potent N-BPs, generates less favourable microenvironment for cancer cell activation in distant organs. For instance, clinical data showed that postmenopausal patients had significantly reduced mortality and less breast cancer recurrence in bones after the treatment (Aft et al., 2010; Coleman et al., 2015). N-BPs also increased expansion of immune cells (Benzaïd et al., 2011; Holmen Olofsson et al., 2021) and caused immunosuppression of regulatory T-cells in breast cancer (Liu et al., 2019).

Macrophages are multifunctional cells in normal physiological homoeostasis and disease pathogenesis. High number of tumour-associated macrophages (TAMs) indicates tumour aggressiveness and poor survival across breast cancer subtypes (Cassetta et al., 2019). Macrophages can adapt a wide spectrum of activation states (Murray and Wynn, 2011; Murray et al., 2014), but conceptually here we use the term “M1” for inflammation augmenting activation states and “M2” for inflammation downregulating / tissue regenerating activation states. In several solid tumours, M1 macrophages have been shown to secrete pro-inflammatory cytokines, express iNOS (Lu et al., 2015; Paul et al., 2019) and associate with tumour suppression (Salmaninejad et al., 2019). In large cohorts of breast cancer (BC) patients, TAMs have been shown to display enriched expression of M2-activation associated genes (Chung et al., 2017). M2-type TAMs probably suppress anti-cancer immunity and secrete growth factors facilitating cancer propagation (Salmaninejad et al., 2019). Macrophages can alter their activation state in response to physiological signals or pharmacological agents. Zoledronate (ZOL), a clinically widely used N-BP, has been shown to promote M1-type macrophage polarization, as indicated by expression of inflammatory cytokines and other inflammation-associated proteins (Kaneko et al., 2018; Zhu et al., 2019).

Due to the BPs high affinity to bone, strategies to achieve high intratumour drug concentrations must be developed for effective TAM modulation. Liposomes (LIP) are lipid bilayer particles, which are widely used preclinically, due to the enhanced permeability and retention effect in tumours (Maruyama, 2011). Formulation of N-BPs by encapsulation in liposomes has been shown to result in better tumour targeting in several solid tumour models, with limited accumulation of drug in normal tissues (La-Beck et al., 2021). For instance, in ovarian cancer liposome-encapsulated alendronate reduced cancer cell viability and tumour growth with increasing expansion of γδ-T cells when compared to alendronate (Parente-Pereira et al., 2014; Hodgins et al., 2016). Liposome formulation of zoledronate (ZOL-LIP) has increased circulation time and lower bone affinity (Shmeeda et al., 2013).

Previously, we showed that ZOL-LIP is up taken by breast cancer cells (Zlatev et al., 2016) and promotes expression of M1 markers in monocyte/ macrophages cultures despite the presence of BC cell secreted factors *in vitro* (Sousa et al., 2015). Moreover, ZOL-LIP reduces monocyte/macrophage infiltration into tumours (Cai et al., 2017). Here, we investigated whether TAM targeted by ZOL-LIP enhances tumour growth inhibition and affects polarization and / or number of macrophages in TNBC tumours, when compared with free ZOL.

2. Materials and methods

2.1. Cell culture

Mouse mammary 4T1 cancer cells (ATCC) were cultured in RPMI-1640 medium and human MDA-MB-231 cancer cells (ATCC) were cultured in DMEM medium (Sigma Aldrich Ltd, St. Louis, MO) supplemented with 10% foetal bovine serum (FBS, Life Technologies Ltd, Carlsbad, CA) and 100 IU/ml penicillin streptomycin (Sigma). Cells were incubated at 37 °C in 5% CO_2. The 4T1 cell labelling was achieved by retroviral transduction using the pmiRVec retroviral vector containing the luciferase2 open reading sequence (Croset et al., 2018). The stably transduced 4T1.luc2 cell line was like the parental line regarding *in vivo* and *in vitro* growth kinetics. Cells were tested for mycoplasma contamination on a regular basis (MycoAlert Mycoplasma detection kit, Lonza, Basel, Switzerland). Luciferase activity was checked prior to injection in mammary fat pads with the EnVision® Multiplate Reader (Perkin Elmer, Turku, Finland), using the One-Glo™ luciferase assay system (Promega, Madison, WI, USA) following manufacturer’s instructions.

2.2. Liposome preparation

Negatively charged empty liposomes (EMP-LIP) and ZOL-LIP were prepared by the reverse-phase evaporation method (Zlatev et al., 2016). Liposome size, lipid and drug contents were analysed as previously described (Mönkkönen et al., 1994; Sousa et al., 2015; Zlatev et al., 2016). Liposome size was between 100 and 200 nm, liposomal ZOL concentration in ZOL-LIP was 1 mM, according to spectrophotometric analysis (Mönkkönen et al., 1994). Liposome stock solutions were diluted in PBS immediately before use by gently mixing.

2.3. Measurement of ApppI accumulation in breast cancer cells

4T1.luc2 cells (1×10^6 cells/well) were plated in 6-well plates and allowed to adhere overnight prior to 24 h zoledronate (ZOL) (Novartis, Switzerland, Basel) and liposome treatments. ApppI amounts were determined in dried acetonitrile/water cell extracts by HPLC-ESI-MS as previously described (Mönkkönen et al., 2000, 2006). Briefly, dried extraction pellets were dissolved in 150 µl of 1 µM internal standard (IS), β,γ-methylene adenosine 5- triphosphate disodium salt (AppCp) (Sigma, Germany) and centrifuged for 10 min at 13,000 RPM 4 °C. HPLC separation was done with an Agilent 1200 HPLC system (Waldbronn, Germany) by using a (30 mm × 3 mm, 2.6 µm) reversed-phase C18 column (Phenomenex, Torrance,CA, USA). The subsequent mass spectometric analysis was done with LTQ ion trap mass spectrometer (San Jose, CA, USA) with following detection parameters *m/z* IPP 245 → 159, ApppI, 574 → 408, and 504 → 406 AppCp. Quantification of the molecules was performed using LCquan 2.0 software (Thermo Scientific, Carlsbad, CA, USA).

2.4. Cell viability assay

4T1 or MDA-MB-231 cells were seeded in 96 well-plates (2×10^3 cells/well) and left to attach overnight. ZOL was added to cells in range 10 – 50 µM. Cell viability was measured after 24 h of treatment by WST-8 assay (Dojindo, Biotop Oy, Denmark). ApppI (0.1 – 1 mM) was added freshly every 24 h for 72 h. Cell viability was measured after 72 h from the first treatment. The level of WST-formazan was measured by Tecan ULTRA Reader (Tecan AG, Austria) at 450 nm.

2.5. Migration assay

For migration assays, the cells were cultured with treatment for 24 h on ImageLock 96-well plates (Essen Bioscience, MI, USA). Scratch wounds were made with the WoundMaker (Essen Bioscience, MI, USA), after which the wells were washed with 1x PBS and filled with the fresh medium without treatment. Images were captured every 6 h during 24 h with the IncuCyte S3 imaging system (Essen Bioscience, MI, USA). IncuCyte 2018B software was used to analyse wound confluences.

2.6. Animals

Female 5 – 6-week-old BALB/c mice (Harlan Laboratories, Horst, Netherlands) were used. All animals were maintained under controlled conditions (temperature 20–21 °C, 30–60% relative humidity and 12 h lighting cycle). They were fed with RM3 ESQC food pellets (Special Diets Services, Witham, UK) and supplied with tap water *ad libitum*. Animal welfare was monitored daily, and the animals were weighed twice a week.

2.7. Orthotopic mammary fat pad inoculation of 4T1.luc2 cells

4T1.luc2 (1×10^5) cells were inoculated orthotopically in the 4th mammary fat pads of BALB/c mice. The mice were then randomized into treatment groups according to the tumour volume to ensure equal tumour burden distribution. In the first experimental setup, intraperitoneal (IP) PBS (vehicle), ZOL (100 μg/kg), EMP-LIP (at a dose with equivalent amount of lipids as the ZOL-LIP dose) and ZOL-LIP (drug amount 100 μg/kg) treatments were given each 4th day until day 25. In the second experimental setup, treatments were intravenously injected (IV) for targeting of disseminated tumour cells from the primary tumours and interacting with TAMs located not only in the primary tumours site but also in metastatic sites. Primary tumours were resected at day 8 after cell inoculation. Buprenorphine hydrochloride was used as analgesic drug (Temgesic: 0.05–0.1 mg/kg) in operation and twice a day 2 days after operation. Mice were followed until day 21. Animal weight and tumour size were measured weekly. Animals were imaged with an *in vivo* bioluminescence imaging system (Perkin Elmer, Waltham, MA, USA). Mice were sacrificed prior to day 21 in case of tumour burden meeting the ethical limit, weight loss superior to 20% of initial body weight or signs of animal suffering.

2.8. In vivo bioluminescence imaging

Prior to imaging, 150 μg/kg of D-luciferin in PBS (Gold Biotechnology, St. Louis, MO) were IP injected and all the animals were anesthetized with 2.5% isoflurane. Mice were imaged using a charge-coupled device camera–based bioluminescence imaging system, IVIS Spectrum (Perkin Elmer, Waltham, MA, USA). Exposure time was 1–300 s, binning 4/8/16, field of view 23 cm, f/stop 1, and emission filter opened. Signal was measured and recorded as total flux (photons/*sec*). Corresponding grey scale photographs and colour luciferase images were automatically superimposed and analysed with Living Image software (PerkinElmer, MA, USA).

2.9. Colony formation assay

4T1 or MDA-MB-231 (500 cells/well) cells were seeded in 6 well-plates and left to attach overnight. On the next day, ZOL was added to cells. After 24 h, fresh complete media without ZOL was added to the plate to allow cells to form colonies.

Tibias and femurs were minced and soaked in an enzyme cocktail containing 300 U/mL type- I collagenase and 100 U/mL hyaluronidase (StemCell Technologies). Lungs were minced and an enzyme solution containing 0.25 mg/mL type-I collagenase (Sigma) was added. Both organ homogenates were incubated for 2 h at 37 °C. After incubation, cell suspensions from bone marrow and lungs were passed through 40 μm cell strainers (Falcon, BD Biosciences), centrifuged 5 min at 1000 rpm. Fresh complete medium was added, and the cell suspensions were seeded in six-well plates for 24 h. The next day, the cells were placed under 6-thioguanine (Sigma) antibiotic selection for two weeks, allowing the selective growth of antibiotic-resistant disseminated tumour cells. Colonies of tumour cells were fixed and stained with crystal violet. Colonies of at least 50 cells were taken in analysis (Franken et al., 2006). Colonies were counted using Fiji-ImageJ (1.52p) software (Schindelin et al., 2012).

2.10. Immunohistochemistry

Formalin-fixed tissue samples from tumours and lungs were embedded in paraffin and cut in 4 μm sections. Dissected tissues were stained by immunohistochemical and immunofluorescence assays. List of antibodies used in experiments is described in Supplementary Table 1. Negative controls were used to verify the specificity of the staining. Slides were scanned using Pannoramic 250 slide scanner (3DHISTECH Ltd, Hungary). Acquired digital slides were analysed with QuPath-0.2.0 software (Bankhead et al., 2017). QuPath scripts for staining analysis are presented in Supplementary Table 2. CD34 staining was analysed in ten hotspots (40x) of total area by using Fiji-ImageJ (1.52p) software. All stainings were evaluated blindly.

2.11. Western blotting

Whole tumour cell lysates were prepared by homogenization of the tissues on ice in RIPA buffer including protease and phosphatase inhibitor cocktail (Thermo Fisher Scientific, USA) with an Ultra-Turrax homogenizer. The homogenates were subsequently centrifuged for 10 min at 13,000 RPM, and the supernatants were collected. The protein amounts were calculated using the BCA protein assay with BSA as standard (Thermo Fisher Scientific). Primary antibodies diluted in 5% dry milk in TBST were incubated overnight at 4 °C. Secondary detection for 1 h at room temperature was performed with fluorescent secondary antibodies conjugated to Alexa Fluor fluorochromes. Antibodies used in Western blotting are listed in the Supplementary Table 1. The emitted fluorescence was detected with Li-Cor Odyssey® CLx imaging system.

2.12. TaqMan RT-qPCR

Total RNA from tumours was isolated with RNeasy RNA isolation kit according to the manufacturer's instructions (Macherey-Nagel, Germany). TaqMan RT-PCR was performed using TaqMan Universal Master Mix II (Thermo Fisher Scientific, USA). TaqMan probes are listed in the Supplementary Table 1. The results were analysed using the delta-delta Ct-method by first adjusting the Ct-values to that of the housekeeping gene encoding ribosomal 18S RNA.

2.13. Bone histomorphometry

Decalcified bones were embedded in paraffin. Osteoclasts were stained with commonly used tartrate-resistant acid phosphatase (TRAcP) method (Merck, Germany). Bone histomorphometry was analysed using TrapHisto software (van 't Hof et al., 2017). The number of osteoclasts were counted per area in the trabecular bone manually using Fiji-ImageJ (1.52p) software (Schindelin et al., 2012).

2.14. Ethics declarations

The animal experiments were carried out according to the European Convention for the Protection of Vertebrate Animals used for Experimental and other Scientific Purposes, and statutes 1076/85 and 1360/90 of The Animal Protection Law in Finland and EU Directive 86/609 and national permissions from the French Government. The experimental procedures were reviewed by the local Ethics Committee on Animal Experimentation of the University of Turku and approved by the local Provincial State Office of Western Finland, permission number ESAVI/3257/04.10.07/2014. We confirm that all methods and experiments were carried out in accordance with relevant guidelines and regulations.

2.15. Statistical analysis

All analyses were performed using GraphPad Prism version 7.0 (GraphPad Software Inc, San Diego, CA, USA). Data were analysed for

statistical significance using Wilcoxon singed-rank test, Mann-Whitney t – test and ANOVA tests; Tukey's; Sidak's post-hoc tests. Shapiro-Wilk test was used as a normality test. Differences for which P was <0.05 are reported as statistically significant. The Mantel-Cox test was used in survival curve comparisons.

3. Results

3.1. Liposome-encapsulated zoledronate increased ApppI accumulation and reduced cancer cell migration

First, we investigated inhibitory effects of ZOL on TNBC cancer cells. ZOL significantly decreased 4T1 and MDA-MB-231 cell viability in comparison to vehicle groups (Fig. 1a, b, $p = 0.029$ for both, respectively). ApppI decreased 4T1 cell viability significantly after 72 h of daily repeated treatment ($p = 0.029$), but not in MDA-MB-231 cells in comparison to vehicle groups (Fig. 1c, d). ZOL significantly reduced the number of colonies after 24 h of treatment in 4T1 and MDA-MB-231 cells in comparison to vehicle groups (Fig. 1e, f, $p = 0.029$ for both, respectively). Formation of metastases in distant organs relies on the ability of cancer cells to migrate. Thus, we tested the effect of ZOL and ZOL-LIP on migration potential of 4T1 cells *in vitro* with wound healing assay. The migration of 4T1 was significantly decreased after ZOL-LIP treatment when compared to ZOL or vehicle groups (Fig. 1g, $p = 0.022$ and 0.008, respectively). Similar trend was seen also for MDA-MB-231 cells (Fig. 1h, $p = 0.0501$). Treatment with ZOL-LIP (5 and 10 μM) led to ApppI accumulation, whereas no ApppI could be detected in ZOL-treated 4T1 cells (Supplementary Fig. 1).

3.2. Liposome-encapsulated zoledronate delayed tumour growth in vivo

The 4T1 orthotopic mouse breast cancer model was used to investigate the *in vivo* effects of ZOL-LIP on tumours (Fig. 2a). Animals received the same amount of drug (100 μg/kg) either as free ZOL or packed in liposomes, ZOL-LIP. ZOL and ZOL-LIP treatment significantly decreased tumour growth in both groups (Fig. 2b, $p = 0.01$ and < 0.001,

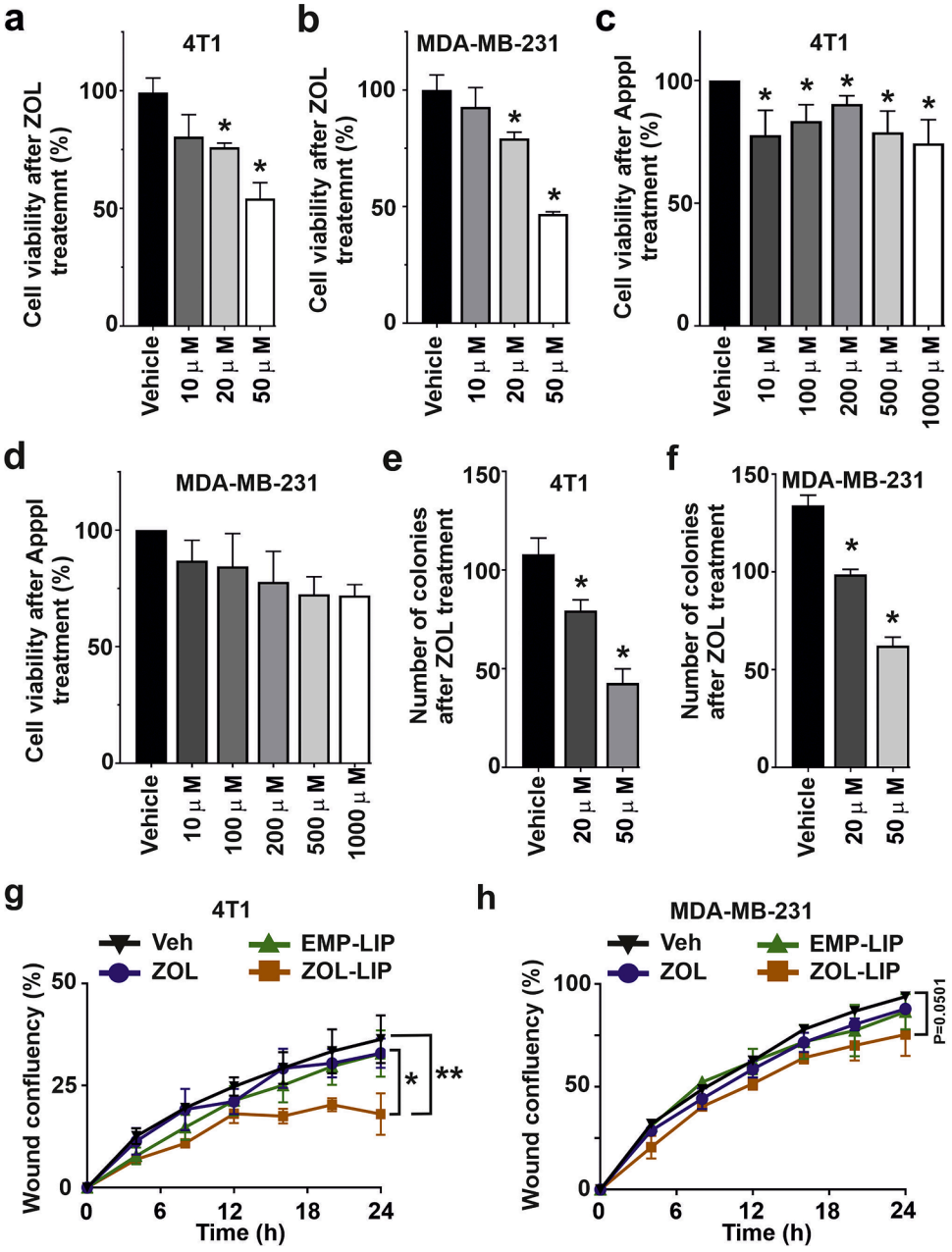

Fig. 1. Effect of liposome-encapsulated zoledronate on ApppI accumulation and 4T1 cell migration. Cell viability after 24 h of ZOL treatment in (a) 4T1 and (b) MDA-MB-231 cells as measured with WST assay. Cell viability after 72 h of ApppI treatment in (c) 4T1 and (d) MDA-MB-231 cells as measured with WST assay. The bars represent fold-change in viability of untreated *vs.* treated cells. Number of cancer cell colonies after 24 h of ZOL treatment in (e) 4T1 and (f) MDA-MB-231 cells. * $P < 0.05$ is considered to be statistically significant compared to control, by Mann-Whitney U test. The results are expressed as mean ± SD, $n = 3$. * $P < 0.05$ is considered to be statistically significant compared to control, by Mann-Whitney U test. Cancer cells scratch-wound assay after 24 h of ZOL or ZOL-LIP treatment in (g) 4T1 and h) MDA-MB-231 cells as measured with IncuCyte 2018B software (Essen Bioscience). The results are expressed as mean ± SD, $n = 3$. * $P < 0.05$; ** $P < 0.01$ are considered to be statistically significant compared to representative controls, by two-way ANOVA with a Tukey's post-test.

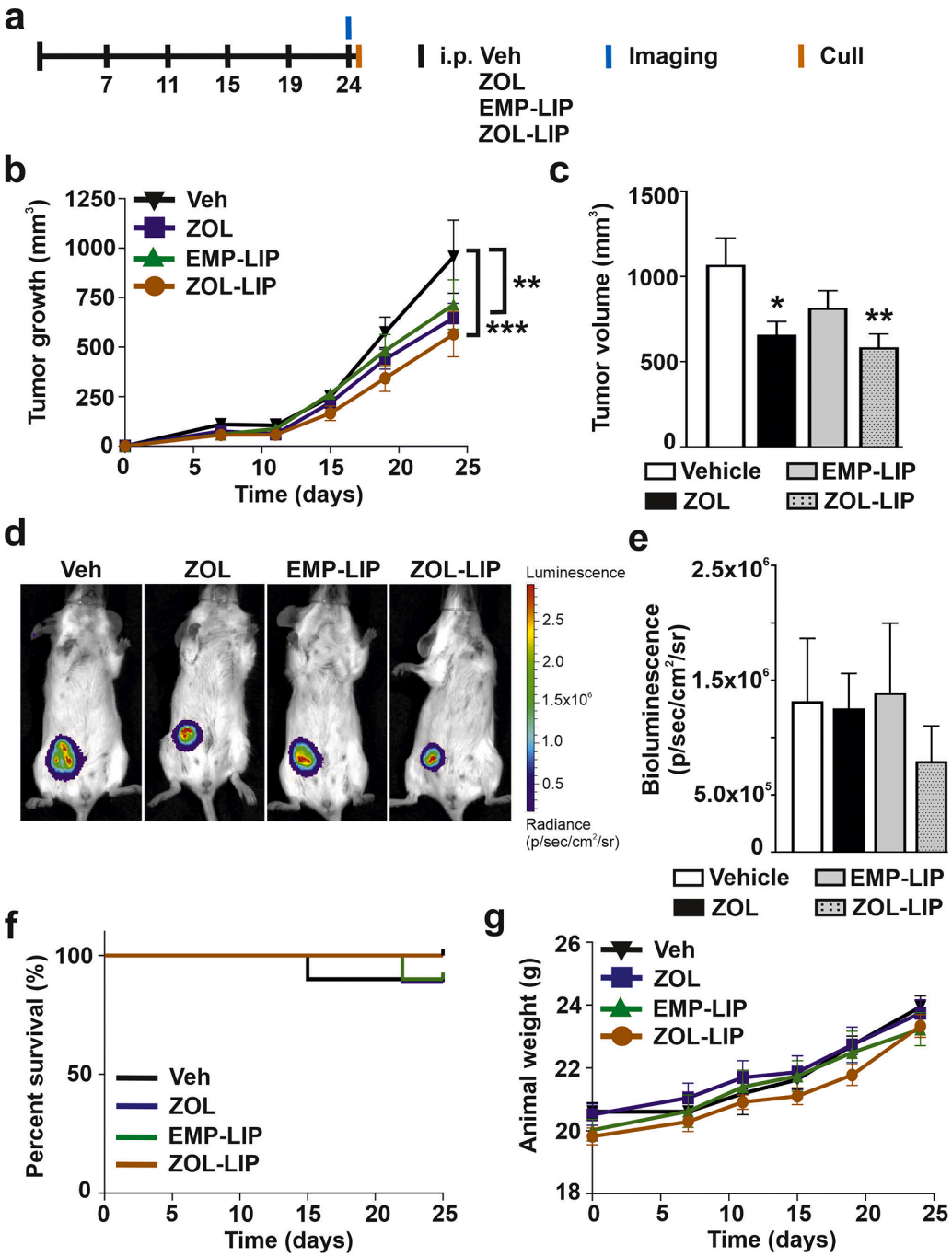

Fig. 2. Effect of liposome-encapsulated zoledronate on tumour growth. (a) Schematic views of *in vivo* experiments with 4T1.luc2 cells inoculated subcutaneously in 4th mammary fat pad (n = 10). (b) 4T1.luc2 tumour growth over 24 days. The results are expressed as mean ± SEM. * $P < 0.05$; ** $P < 0.01$ are considered to be statistically significant compared to representative controls, by two-way ANOVA with a Tukey's post-test. (c) Post-mortem tumour volume. The results are expressed as mean ± SEM, * $P < 0.05$; ** $P < 0.01$ are considered to be statistically significant compared to control, by Mann-Whitney U test. (d) Representative bioluminescence images of tumours at day 24. (e) Bioluminescence image analysis of tumour burden at day 24. (f) Survival of treatment groups. The Mantel-Cox test was used in survival curve comparisons. (g) Animal weight of mice during 24 days of treatment.

respectively). At sacrifice, tumours of ZOL and ZOL-LIP groups were significantly smaller (32% and 41%, $p = 0.011$ and 0.008, respectively) than those in vehicle group (Fig. 2c). In line with decreased tumour volume, for tumours in the ZOL-LIP group bioluminescence trended to be lower when compared with PBS or ZOL groups (Fig. 2d, e). All animals treated with ZOL-LIP survived (Fig. 2f). Treatments did not affect animal weight (Fig. 2g). Although, we did not observe macro-metastases in distant organs, using the *in vivo* imaging system, the presence of cancer cells in lung and bones were detected in colony formation assays (Supplementary Fig. 1). ZOL and ZOL-LIP treatments appeared to reduce tumour cell colony formation in lungs, but this decrease was not statistically significant. Moreover, there was no major treatment effect on the number of tumour cell colonies isolated from bones (Supplementary Fig. 1). In addition to accumulation of ApppI in cancer cells, N-BPs treatment leads to inhibition of protein prenylation (Okamoto et al., 2014; Munoz et al., 2021). We showed that ZOL slightly increased accumulation of unprenylated Rab4, whereas ZOL-LIP lead to its significant accumulation in tumours compared to controls (Supplementary Fig. 2), indicating intra-tumour targeting of ZOL. Thus, ZOL-LIP treatment more efficiently targeted TNBC tumours than ZOL treatment.

3.3. ZOL-LIP effect on macrophages at the early stage of the tumour growth phase

Tumour growth monitoring suggested that tumours grew in two phases: an early growth phase until day 12 post-inoculation and then a late accelerated growth phase at day 12 post-inoculation (Fig. 2b). To investigate the effect of short-term ZOL-LIP treatment on macrophage infiltration, we resected tumours on day 8 before the accelerated growth phase (Fig. 3a). Tumour bioluminescence at day 4 trended to be lower

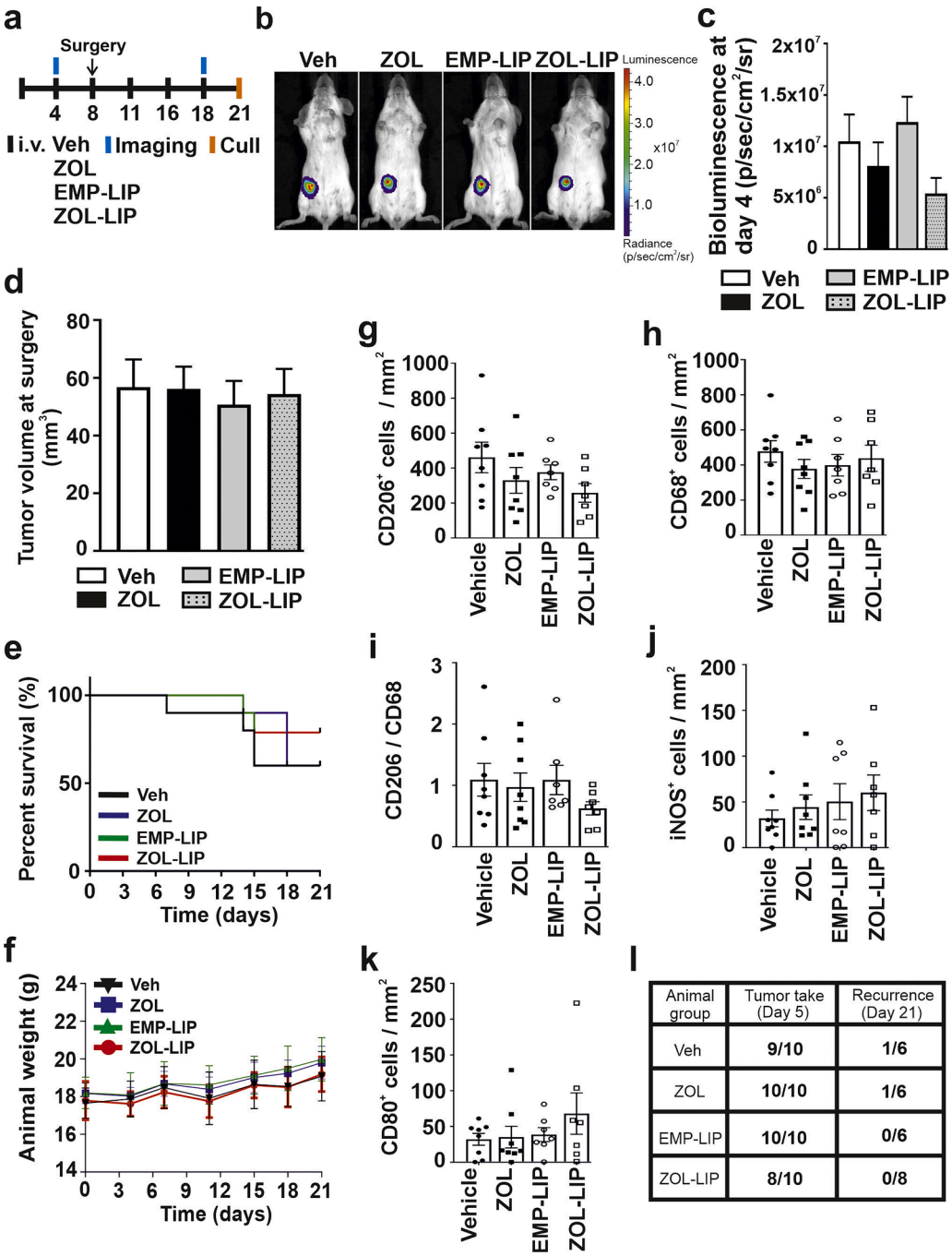

l

Animal group	Tumor take (Day 5)	Recurrence (Day 21)
Veh	9/10	1/6
ZOL	10/10	1/6
EMP-LIP	10/10	0/6
ZOL-LIP	8/10	0/8

Fig. 3. Effect of liposome-encapsulated zoledronate on tumour radiance and macrophage number in a slow tumour growth phase. (a) Schematic views of *in vivo* experiments with 4T1.luc2 tumour resection (n = 10). IV: intravenously. (b) Representative bioluminescence images of tumours at day 4. (c) Bioluminescence image analysis of tumour burden at day 4. (d) Tumour volume at surgery. (e) Survival of treatment groups. The Mantel-Cox test was used in survival curve comparisons. (f) Animal weight of mice during 21 days of treatment. Number of (g) CD206 and (h) CD68 positive cells. (i) Ratio of CD206/CD68 positive cells. Number of (j) iNOS and k) CD80 positive cells. Each symbol represents an individual animal. (l) 4T1.luc2 cell tumour take and recurrence rate. The numbers indicate formed tumours per 10 tumour inoculations. The results are expressed as mean ± SEM.

upon ZOL and ZOL-LIP treatment in comparison to control groups (Fig. 3b, c). Treatment did not affect the tumour formation at the day of resection (Fig. 3d). We observed a trend in better animal survival upon ZOL-LIP in comparison to the vehicle group, but it did not reach significance (Fig. 3e, 80% *vs* 60% ZOL-LIP *vs* vehicle). The treatment did not affect body weight (Fig. 3f). There was a trend towards decreased $CD206^+$ cell numbers ("M2" macrophage marker) in ZOL and ZOL-LIP groups when compared to controls (Fig. 3g). Treatments did not have an obvious effect on $CD68^+$number (pan-macrophage marker) and the mean CD206/CD68 expression ratio in tumours during the early growth phase (Fig. 3h, i). There was a trend towards increased number of $iNOS^+$and $CD80^+$ ("M1" macrophage marker) cells in the ZOL-LIP group (Fig. 3j, k). At the end of experiment, tumour recurrence was observed in vehicle and ZOL groups (Fig. 3l).

3.4. Liposome-encapsulated zoledronate increased the shift towards M1-like TAM polarization in primary TNBC tumours in the accelerated growth phase

Next, we investigated whether the long-term ZOL-LIP treatment altered the number of macrophages in tumours in the accelerated growth phase. Animals without tumour resection were followed for 25 days. The number of $CD206^+$ macrophages was significantly decreased in tumours upon ZOL-LIP treatment when compared to the vehicle group (p = 0.035). Instead, ZOL showed only a similar trend (Fig. 4b). The number of $CD68^+$macrophages was significantly increased (p = 0.020) and CD206/CD68 ratio decreased (p = 0.001) in the ZOL-LIP group when compared to the vehicle group (Fig. 4c and 4 d, respectively). ZOL treatment showed similar trend on this transition (Fig. 4d). Furthermore, there was a trend for high expression of $iNOS^+$ cells in tumours of

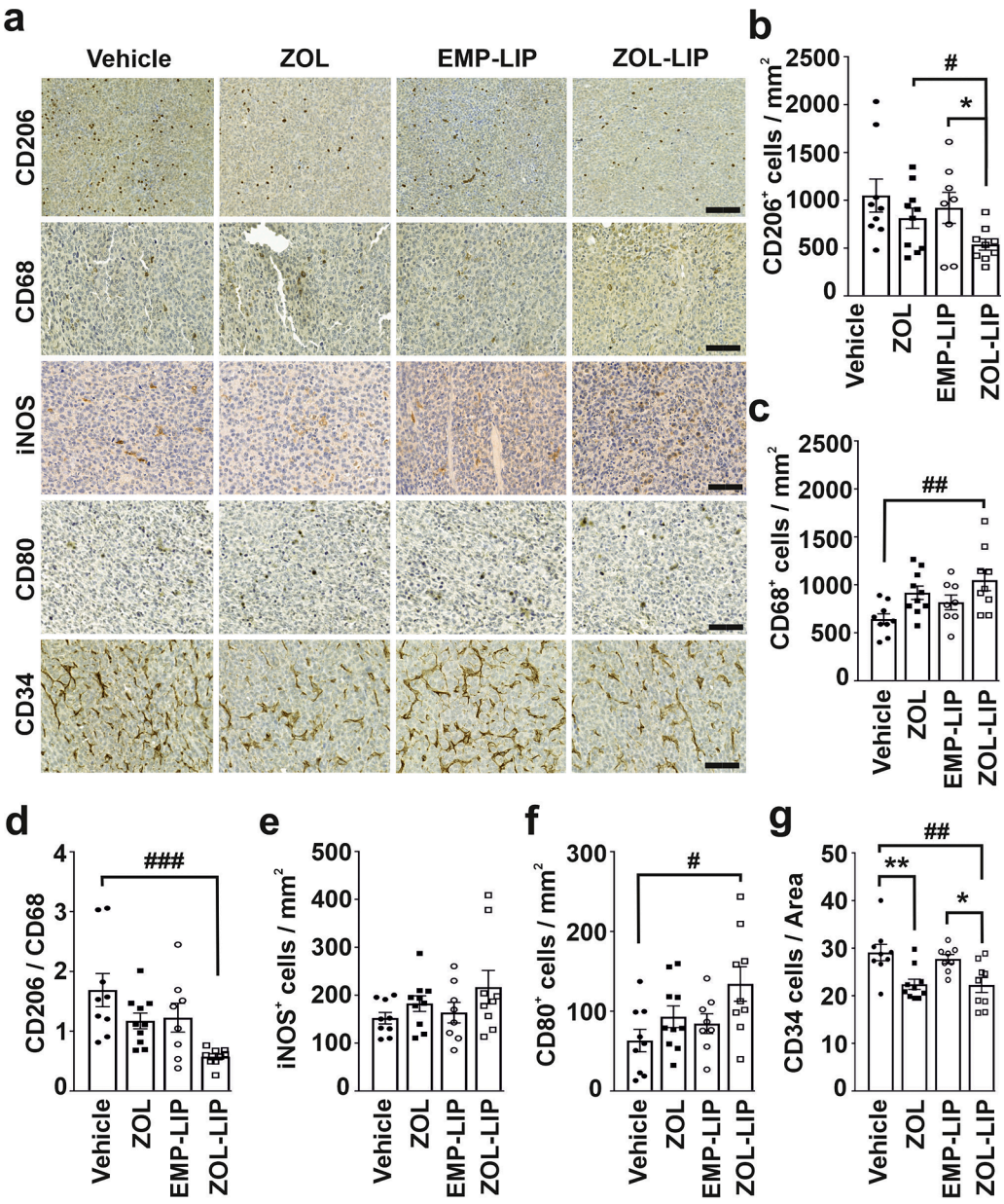

Fig. 4. Effect of liposome-encapsulated zoledronate on TAMs number and CD34 expression in primary TNBC tumours. (a) Representative images of tumour staining. Scale bar = 100 μm. Scale bar 200 μm for CD206. Number of (b) CD206, (c) CD68 (d) Ratio of CD206/CD68 positive cells. (e) Expression of iNOS in tumours. (f) Number of CD80 positive cells. (g) Expression of CD34 in tumour area. Immunohistochemical staining expressions were quantified by QuPath. Each symbol represents individual animal. Data is expressed as mean ± SEM, * $P < 0.05$; # $P < 0.05$, $n = 8 – 10$; are considered to be statistically significant compared to the respective controls, by one-way ANOVA with Sidak's post-test.

the ZOL-LIP group when compared to vehicle (Fig. 4e). The number of $CD80^+$cells was significantly increased in tumours upon ZOL-LIP treatment in comparison to vehicle group (Fig. 4f, $p = 0.01$). ZOL and ZOL-LIP significantly decreased CD34 expression (Fig. 4g, $p = 0.004$ for both, respectively). Our results indicated that ZOL-LIP treatment led to an enhanced macrophage shift towards M1 phenotype in TNBC tumours. Additionally, although there was only a trend for increased $CD3^+$ and $CD8^+$ T cell infiltration into tumours in ZOL and ZOL-LIP treated groups (Fig. 5, a–c), infiltration of $CD4^+$ T cells was significantly increased upon ZOL-LIP compared to vehicle ($p = 0.026$) or EMP-LIP ($p = 0.011$) groups (Fig. 5a, d).

3.5. Liposome-encapsulated zoledronate induced expression of cytokines and inflammatory transcription factors in tumour tissue

Next, we investigated whether the increased proportion of M1-like macrophages and iNOS expression is reflected in the expression of inflammation-regulating transcription factors and cytokines in tumours on the accelerated growth stage. NF-κB protein level was significantly increased in ZOL-LIP group in comparison to EMP-LIP ($p = 0.012$), (Fig. 5e, f and Supplementary Figs. 2, 3). There was a trend towards decreased protein level of p-IκBα in ZOL group and increased p-IκBα in ZOL-LIP group when compared to corresponding control groups (Fig. 5e, g and Supplementary Figs. 2, 3). Small increase of the mean mRNA level of inflammatory cytokines IL-1β and IL-6 in tumours was seen upon ZOL and ZOL-LIP treatment (Fig. 5h, i). Although, we did not see significant difference in IL-1 and IL-6, the trend in the mean expression values is consistent with the effects in the NF-kB expression. No effect was detected on IL-10 mRNA expression in tumours (Fig. 5j).

3.6. Effect of liposome-encapsulated zoledronate on osteoclasts and bone resorption

Increased activity in non-bone tissues suggests that liposome encapsulation may have altered ZOL distribution in soft tissues when compared to conventional ZOL formulation, which has high affinity to bones. ZOL-LIP treatment significantly decreased the total number of osteoclasts / area (N.Oc. / T.Ar) ($p = 0.047$), whereas the effect of ZOL

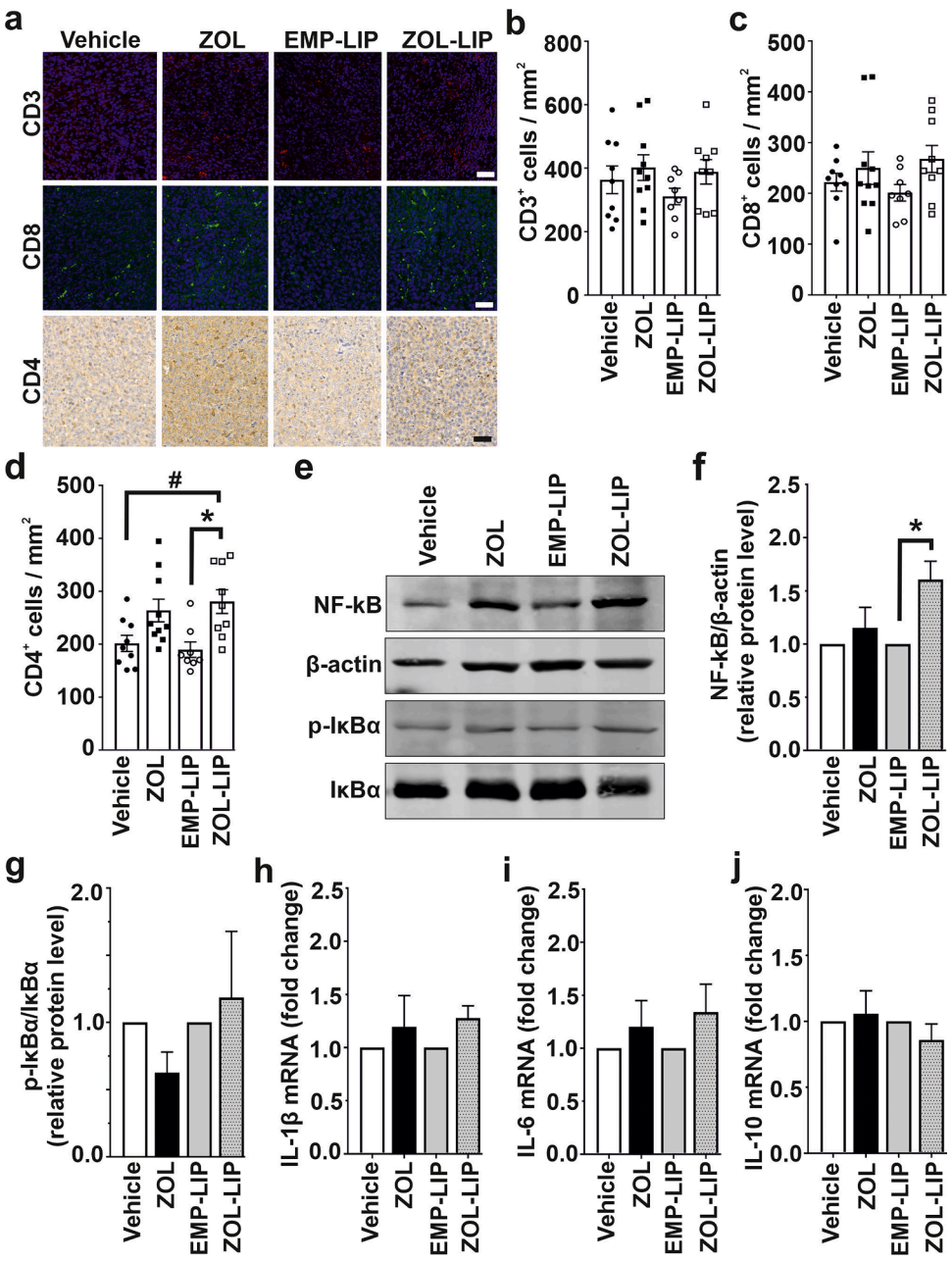

Fig. 5. Effect of liposome-encapsulated zoledronate on cytokines expression and inflammatory transcription factors in tumour tissue. (a) Representative images of tumour staining. Scale bar = 100 μm. Number of (b) CD3 (c) CD8 (d) CD4 positive cells in tumours. (e) Representative blots of protein expression in tumour tissues. Fold change of protein expression of (f) NF-κB and (g) phosphorylated-IκBα in tumour tissues. mRNA level of (h) IL-1β, (i) IL-6 and (j) IL-10 in tumour tissues. The results are expressed as mean ± SEM, each symbol represents individual animal. * $P < 0.05$ are considered to be statistically significant compared to the respective controls, by Wilcoxon singed-rank test.

was not significant when compared to respective controls (Fig. 6a, b). However, the number of osteoclasts per bone volume (N.Oc./BV) were significantly reduced both in ZOL and ZOL-LIP groups when compared to respective controls ($p = 0.003$ and < 0.001, respectively) (Fig. 6c). In line with the effects on N.Oc, ZOL and ZOL-LIP significantly increased BV when compared to controls. However, the anabolic effect on BV was significantly smaller in ZOL-LIP group when compared to ZOL group ($p = 0.036$) (Fig. 6d). BV/TV ratio was significantly increased only in ZOL group compared to controls ($p = 0.027$) (Fig. 6e). Taken together, this suggests that liposome encapsulation of ZOL slightly reduces the bone anabolic effects of ZOL.

4. Discussion

Mevalonate pathway is a biosynthesis process that produces cholesterol and intermediate isoprenoids important for protein prenylation. Its products are involved in facilitating cancer cells proliferation, tumour progression and resistance to chemotherapy (Sethunath et al., 2019). Inhibition of farnesyl pyrophosphate synthase of the mevalonate pathway by N-BPs lead to accumulation of IPP and ApppI which can have pleiotropic effects on tumours in addition to direct cytotoxicity. For example, anti-cancer immunity may be enhanced by activation of γδ-T cells (Parente-Pereira et al., 2014). Nitrogen-containing bisphosphonates have been demonstrated to be an effective adjuvant as well as neoadjuvant therapy for postmenopausal women with breast cancer (Coleman et al., 2015; Kroep et al., 2016; Rennert et al., 2017; Strobl et al., 2018). However, the therapeutic use of N-BPs in the treatment of cancer has remained limited due to side effects (Seider et al., 2018; Gralow et al., 2020). Bisphosphonate encapsulation in liposomes may allow to reduce drug dosing with better tumour targeting (La-Beck et al., 2021). For instance, as shown by Shmeeda et al. (2013), the biodistribution of zoledronate was radically modified by liposome encapsulation, increasing spleen and liver accumulation by 20–100-fold, tumour accumulation in lung carcinoma by 7–10-fold and bone accumulation by 2-fold in mice. In the same study, a non-cumulative lethal ZOL-LIP toxicity was found. This seemed to be

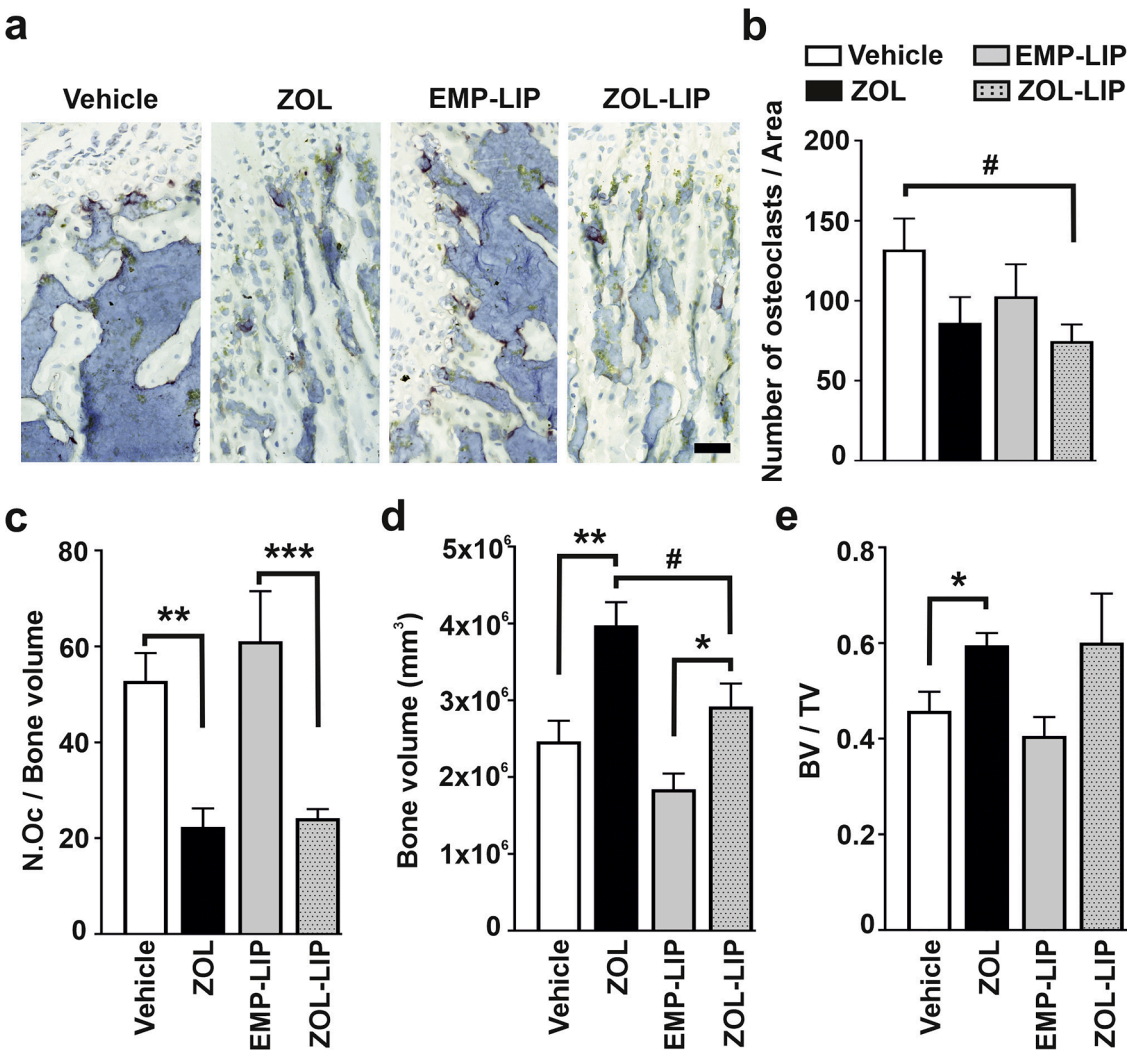

Fig. 6. Effect of liposome-encapsulated zoledronate on osteoclasts and bone resorption. (a) Representative images of TRAcP staining of tibia. Scale bar = 50 μm. (b) Number of osteoclasts below growth plate per area in tibia. (c) Number of osteoclasts per bone volume in tibia. (d) bone volume (e) ratio of bone volume to tissue volume in tibia. The results are expressed as mean ± SEM, * $P < 0.05$; ** $P < 0.01$; # $P < 0.05$ are considered to be statistically significant compared to the respective controls, by one-way ANOVA with a Sidak's post-test.

due to the high dose of ZOL (ZOL-LIP 30 μg/mouse). In our study, we used clinically achievable doses of treatment (100 μg/kg body weight, approximately 2 μg/mouse, which is equivalent to a clinical dose of 4 mg) (Ottewell et al., 2008), which significantly reduced tumour growth and promoted inflammatory activation of TAMs without lethal toxicity. However we did observe occasional splenomegaly (one / group) in ZOL-LIP and EMP-LIP mice, which may indicate some toxicity as seen earlier with liposomal formulations (Sousa et al., 2015), but can be unrelated to the treatment as there was no consistency. Based on the effects in BV, the overall anabolic effect on bone was slightly reduced in ZOL-LIP group when compared to the ZOL group. However, the N.Oc was still reduced in the ZOL-LIP group. These effects might be not just due to the accumulation of ZOL in osteoclasts via resorption but rather due to the capability of osteoclasts and osteoclast precursors to phagocytize ZOL-LIP in bones. This would require more experimentation and long-term follow up with treatment by both formulations.

Tumour-associated macrophages are significant infiltrates in breast tumour microenvironment and due to their immunosuppressive properties (particularly of the M2-type TAMs) they usually correlate with poor prognosis and worse relapse-free survival (Cassetta et al., 2019; Mehta et al., 2021). In TNBC, an M2-type TAM enriched gene signature had also inflammatory and angiogenic properties (Bao et al., 2021). We investigated the dose-dependant effect of ZOL or ZOL-LIP on macrophages in the early slow tumour growth phase and the later accelerated phase. Although we could not observe significant changes in TAM phenotype based on expression of CD206 at the slow tumour growth phase, there was a trend of reduction of the number of $CD206^+$ cells in tumours after only one dose of the ZOL and ZOL-LIP. We and others have previously shown that ZOL-LIP induced pro-inflammatory activation and M1-type polarization of macrophages *in vitro* (Sousa et al., 2015; Kaneko et al., 2018). ZOL-LIP formulation enhances cytotoxicity on macrophages (Sousa et al., 2015), but these *in vitro* cytotoxic concentrations (IC50 1 μM) are not reached in mice in this study (concentration about 0.4 μM). However, local accumulation of the liposomal formulation in tumours may have yielded also cytotoxicity in our experiments. In this study, ZOL-LIP significantly increased the number of CD68 macrophages in tumours when compared to ZOL. iNOS expression is important for M1-type macrophage activation (Lu et al., 2015) and is considered a marker of these pro-inflammatory macrophages (Lisi et al., 2017; Paul et al., 2019). The expression of iNOS and CD80 was further increased by ZOL-LIP when compared to ZOL treatment. Breast cancer patients with increased CD34 expression (angiogenic marker) have higher risk of bone metastasis (Sun et al., 2018). Therefore, the low expression of angiogenic markers might associate with better outcomes

for breast cancer patients (Guarischi-Sousa et al., 2019; Madu et al., 2020). Our results showed that ZOL-LIP treated tumours had fewer $CD206^+$ (M2-type) cells and both ZOL and ZOL-LIP reduced CD34 expression, which indicates reduced angiogenesis.

Cytokines play an essential role in cancer progression. Several studies have demonstrated that N-BP treatment activates γδ T-cells to release inflammatory cytokines (Hewitt et al., 2005; Tanaka et al., 2017, 2018; Hoeres et al., 2018). Activation of NF-κB requires IκBα expression (Mathes et al., 2008). In our study we showed that ZOL-LIP increased NF-κB protein levels in tumour tissue and reduced the relative amount of IκBα. These changes indicate enhanced intratumoural inflammation and, thus, more M1-like activation of macrophages upon ZOL-LIP treatment. It has been previously shown that tumour cells uptake N-BP that leads to accumulation of IPP/ApppI. In the cell culture experiment, only low levels of cytotoxicity were seen with ectopic ApppI. This may be attributed to the instability of ApppI (Jauhiainen et al., 2009). However, ApppI level was detectable in tumours 48 h after the drug was injected last time, but not after 24 h (Benzaïd et al., 2011, 2012). In this study, ApppI was not detected in 4T1 cells upon free ZOL treatment although cytotoxic effects were seen. It may be that very low amounts of ApppI produced within cancer cells were responsible for the effects seen with free ZOL. N-BPs can be taken up not only by tumour cells, but also by tumour macrophages (Junankar et al., 2015). ZOL uptake by macrophages has been shown to inhibit prenylation of small Rab GTPases and accumulation of their unprenylated forms (Okamoto et al., 2014; Ali et al., 2015; Munoz et al., 2021). In our previous study, ZOL-LIP inhibited prenylation of Rap1A almost equally to ZOL in macrophages *in vitro* (Sousa et al., 2015). Here, *in vivo* ZOL-LIP significantly increased Rab4 accumulation in tumours. Collectively, these results point to an enhanced *in vivo* intratumoural accumulation of ZOL, once the drug is liposome encapsulated.

One limitation of this study was due to the small tumour size in the slow growth phase. We were unable to investigate the protein or mRNA levels of inflammatory markers. We used the whole tumour to demonstrate the effect of short term ZOL treatment on macrophage infiltration.

In addition to large clear cell colonies there were numerous small light-blue dots seen in the cell culture wells stained for the colony-formation assay. The presence of numerous smaller aggregations (for an unknown reason) upon ZOL and ZOL-LIP contributed to an apparent increase in the overall surface complexity that could give the impression that treated wells had more colonies in comparison to vehicle. However, they were not considered as colonies as their size do not reach the criteria for colony definition. A colony should include at least 50 cells (Franken et al., 2006).

In conclusion, liposome encapsulation of N-BP is indicated to improve cancer cell targeting. Here, the encapsulation of ZOL into liposomes shifted its effect from a bone anabolic to an anti-tumour response, when compared to that observed with free ZOL. Our results show that the accumulation of N-BPs over time is necessary to achieve intratumoural changes. Thus, N-BP liposomal formulation might minimize drug toxicity in healthy tissues, reducing adverse effects. Our work demonstrates that ZOL-LIP accumulation changes CD68/CD206 ratio and increases the expression of inflammation regulating transcription factors, thus, indicating augmented tumour inflammation in the accelerated growth phase. ZOL treatment without encapsulation did not affect these events, except decreasing a number of CD34 positive cells. However, further studies are needed to fully understand the impact of ZOL-LIP not only on TAMs but also other tumour microenvironment cells.

Funding

The current research was funded by the Seventh Framework Programme (FP7/2007–2013) under grant agreement no.264817 – BONENET (PC, JMö), Turku University Foundation, decision 488/211/2014 (JMä), and by the Academy of Finland, decision number 132389 (JMö).

CRediT authorship contribution statement

Nataliia Petruk: Investigation, Formal analysis, Visualization, Writing – original draft, Writing – review & editing. **Sofia Sousa:** Investigation, Formal analysis, Visualization, Writing – original draft, Writing – review & editing. **Martine Croset:** Writing – review & editing. **Lauri Polari:** Investigation, Writing – review & editing. **Hristo Zlatev:** Investigation, Writing – review & editing. **Katri Selander:** Methodology, Writing – review & editing. **Jukka Mönkkönen:** Writing – review & editing. **Philippe Clézardin:** Methodology, Writing – review & editing. **Jorma Määttä:** Conceptualization, Supervision, Methodology, Formal analysis, Writing – review & editing.

Declaration of Competing Interest

The authors declare that they have no competing interests.

Data availability

Data will be made available on request.

Acknowledgement

Zoledronate was generously donated by Novartis, Switzerland. The authors acknowledge Dr R. Agami (The Netherlands Cancer Institute, Amsterdam, The Netherlands) for the generous gift of pMirVec plasmid. The authors thank Sandra Geraci, Université Claude Bernard-Lyon, Sanni Tuominen and Jaakko Lehtimäki, both from University of Turku, for excellent technical aid. The authors acknowledge the personnel of the Turku center for Disease modelling and of the Animaleries Lyon Est conventionnelles and SPF of the Université Claude Bernard-Lyon for their valuable help. The authors honour the memorial of our colleague and breast cancer researcher Dr. Johanna Tuomela who passed away during this research. Johanna mentored this research and contributed to planning of animal experimentation.

Supplementary materials

Supplementary material associated with this article can be found, in the online version, at doi:10.1016/j.ejps.2023.106571.

References

Aft, R., et al., 2010. Effect of zoledronic acid on disseminated tumour cells in women with locally advanced breast cancer: an open label, randomised, phase 2 trial. Lancet Oncol. 11 (5) https://doi.org/10.1016/S1470-2045(10)70054-1.

Ali, N., et al., 2015. A highly sensitive prenylation assay reveals *in vivo* effects of bisphosphonate drug on the Rab prenylome of macrophages outside the skeleton. Small GTPases 6 (4). https://doi.org/10.1080/21541248.2015.1085485.

Bankhead, P., et al., 2017. QuPath: open source software for digital pathology image analysis. Sci. Rep. 7 (1), 1–7. https://doi.org/10.1038/s41598-017-17204-5.

Bao, X., et al., 2021. Integrated analysis of single-cell RNA-seq and bulk RNA-seq unravels tumour heterogeneity plus M2-like tumour-associated macrophage infiltration and aggressiveness in TNBC. Cancer Immunol. Immunother. 70 (1) https://doi.org/10.1007/s00262-020-02669-7.

Benzaïd, I., et al., 2011. High phosphoantigen levels in bisphosphonate-treated human breast tumors promote Vγ9Vδ2 T-cell chemotaxis and cytotoxicity *in vivo*. Cancer Res. 71 (13) https://doi.org/10.1158/0008-5472.CAN-10-3862.

Benzaïd, I., et al., 2012. *In vivo* phosphoantigen levels in bisphosphonate-treated human breast tumors trigger Vγ9Vδ2 T-cell antitumor cytotoxicity through ICAM-1 engagement. Clin. Cancer Res. 18 (22) https://doi.org/10.1158/1078-0432.CCR-12-0918.

Cai, X.J., et al., 2017. Anti-angiogenic and anti-tumor effects of metronomic use of novel liposomal zoledronic acid depletes tumor-associated macrophages in triple negative breast cancer. Oncotarget 8 (48). https://doi.org/10.18632/oncotarget.20539.

Cassetta, L., et al., 2019. Human tumor-associated macrophage and monocyte transcriptional landscapes reveal cancer-specific reprogramming, biomarkers, and therapeutic targets. Cancer Cell 35 (4). https://doi.org/10.1016/j.ccell.2019.02.009.

Chung, W., et al., 2017. Single-cell RNA-seq enables comprehensive tumour and immune cell profiling in primary breast cancer. Nat. Commun. 8 https://doi.org/10.1038/ncomms15081.
Coleman, R., et al., 2015. Adjuvant bisphosphonate treatment in early breast cancer: meta-analyses of individual patient data from randomised trials. Lancet North Am. Ed. 386 (10001), 1353–1361. https://doi.org/10.1016/S0140-6736(15)60908-4.
Croset, M. et al. (2018) 'MicroRNA-30 family members inhibit breast cancer invasion, osteomimicry, and bone destruction by directly targeting multiple bone metastasis-associated genes', in. doi: 10.1158/1538-7445.am2018-486.
Franken, N.A.P., et al., 2006. Clonogenic assay of cells *in vitro*. Nat. Protoc. 1 (5) https://doi.org/10.1038/nprot.2006.339.
Gralow, J.R., et al., 2020. Phase III randomized trial of bisphosphonates as adjuvant therapy in breast cancer: S0307. J. Natl. Cancer Inst. 112 (7) https://doi.org/10.1093/jnci/djz215.
Guarischi-Sousa, R., et al., 2019. A transcriptome-based signature of pathological angiogenesis predicts breast cancer patient survival. PLoS Genet. 15 (12) https://doi.org/10.1371/journal.pgen.1008482.
Hewitt, R.E., et al., 2005. The bisphosphonate acute phase response: rapid and copious production of proinflammatory cytokines by peripheral blood γδ T cells in response to aminobisphosphonates is inhibited by statins. Clin. Exp. Immunol. 139 (1) https://doi.org/10.1111/j.1365-2249.2005.02665.x.
Hodgins, N.O., et al., 2016. *In vitro* potency, *in vitro* and *in vivo* efficacy of liposomal alendronate in combination with γδ T cell immunotherapy in mice. J. Control. Release 241. https://doi.org/10.1016/j.jconrel.2016.09.023.
Hoeres, T., et al., 2018. Improving the efficiency of Vγ9Vδ2 T-cell immunotherapy in cancer. Front. Immunol. https://doi.org/10.3389/fimmu.2018.00800.
Holmen Olofsson, G., et al., 2021. The capacity of CD4+ Vγ9Vδ2 T cells to kill cancer cells correlates with co-expression of CD56. Cytotherapy 23 (7). https://doi.org/10.1016/j.jcyt.2021.02.003.
Jauhiainen, M., et al., 2009. Analysis of endogenous ATP analogs and mevalonate pathway metabolites in cancer cell cultures using liquid chromatography-electrospray ionization mass spectrometry. J. Chromatogr. B Anal. Technol. Biomed. Life Sci. 877 (27) https://doi.org/10.1016/j.jchromb.2009.07.010.
Junankar, S., et al., 2015. Real-time intravital imaging establishes tumor-associated macrophages as the extraskeletal target of bisphosphonate action in cancer. Cancer Discov. 5 (1) https://doi.org/10.1158/2159-8290.CD-14-0621.
Kaneko, J., et al., 2018. Zoledronic acid exacerbates inflammation through M1 macrophage polarization. Inflamm. Regen. 38 (1) https://doi.org/10.1186/s41232-018-0074-9.
Kroep, J.R., et al., 2016. Effects of neoadjuvant chemotherapy with or without zoledronic acid on pathological response: a meta-analysis of randomised trials. Eur. J. Cancer 54. https://doi.org/10.1016/j.ejca.2015.10.011.
La-Beck, N.M., et al., 2021. Repurposing amino-bisphosphonates by liposome formulation for a new role in cancer treatment. Semin. Cancer Biol. https://doi.org/10.1016/j.semcancer.2019.12.001.
Lisi, L., et al., 2017. Expression of iNOS, CD163 and ARG-1 taken as M1 and M2 markers of microglial polarization in human glioblastoma and the surrounding normal parenchyma. Neurosci. Lett. 645. https://doi.org/10.1016/j.neulet.2017.02.076.
Liu, H., et al., 2019. Zoledronic acid blocks the interaction between breast cancer cells and regulatory T-cells. BMC Cancer 19 (1). https://doi.org/10.1186/s12885-019-5379-9.
Lu, G., et al., 2015. Myeloid cell-derived inducible nitric oxide synthase suppresses M1 macrophage polarization. Nat. Commun. 6 https://doi.org/10.1038/ncomms7676.
Madu, CO., et al., 2020. Angiogenesis in breast cancer progression, diagnosis, and treatment. J. Cancer. https://doi.org/10.7150/jca.44313.
Maruyama, K., 2011. Intracellular targeting delivery of liposomal drugs to solid tumors based on EPR effects. Adv. Drug Deliv. Rev. https://doi.org/10.1016/j.addr.2010.09.003.
Mathes, E., et al., 2008. NF-κB dictates the degradation pathway of IκBα. EMBO J. 27 (9) https://doi.org/10.1038/emboj.2008.73.
Mehta, A.K., et al., 2021. Macrophage biology and mechanisms of immune suppression in breast cancer. Front. Immunol. https://doi.org/10.3389/fimmu.2021.643771.
Mitrofan, L.M., Pelkonen, J., Mönkkönen, J., 2009. The level of ATP analog and isopentenyl pyrophosphate correlates with zoledronic acid-induced apoptosis in cancer cells *in vitro*. Bone 45 (6). https://doi.org/10.1016/j.bone.2009.08.010.
Mönkkönen, H., et al., 2000. Analysis of an adenine nucleotide-containing metabolite of clodronate using ion pair high-performance liquid chromatography-electrospray ionisation mass spectrometry. J. Chromatogr. B Biomed. Sci. Appl. 738 (2) https://doi.org/10.1016/S0378-4347(99)00559-9.
Mönkkönen, H., et al., 2006. A new endogenous ATP analog (ApppI) inhibits the mitochondrial adenine nucleotide translocase (ANT) and is responsible for the apoptosis induced by nitrogen-containing bisphosphonates. Br. J. Pharmacol. 147 (4) https://doi.org/10.1038/sj.bjp.0706628.
Mönkkönen, J., et al., 1994. Growth inhibition of macrophage-like and other cell types by liposome-encapsulated, calcium-bound, and free bisphosphonates *in vitro*. J. Drug Target 2 (4). https://doi.org/10.3109/10611869409015910.
Munoz, M.A., et al., 2021. Bisphosphonate drugs have actions in the lung and inhibit the mevalonate pathway in alveolar macrophages. eLife 10. https://doi.org/10.7554/eLife.72430.
Murray, P.J., et al., 2014. Macrophage activation and polarization: nomenclature and experimental guidelines. Immunity. https://doi.org/10.1016/j.immuni.2014.06.008.
Murray, P.J., Wynn, T.A., 2011. Protective and pathogenic functions of macrophage subsets. Nat. Rev. Immunol. https://doi.org/10.1038/nri3073.
Okamoto, S., et al., 2014. Zoledronic acid induces apoptosis and S-phase arrest in mesothelioma through inhibiting Rab family proteins and topoisomerase II actions. Cell Death Dis. https://doi.org/10.1038/cddis.2014.475.
Ottewell, P.D., et al., 2008. Antitumor effects of doxorubicin followed by zoledronic acid in a mouse model of breast cancer. J. Natl. Cancer Inst. 100 (16) https://doi.org/10.1093/jnci/djn240.
Parente-Pereira, A.C., et al., 2014. Adoptive immunotherapy of epithelial ovarian cancer with Vγ9Vδ2 T cells, potentiated by liposomal alendronic acid. J. Immunol. 193 (11) https://doi.org/10.4049/jimmunol.1402200.
Paul, S., et al., 2019. Natural killer T cell activation increases iNOS+CD206- M1 macrophage and controls the growth of solid tumor. J. Immunother. Cancer 7 (1). https://doi.org/10.1186/s40425-019-0697-7.
Rennert, G., et al., 2017. Oral bisphosphonates and improved survival of breast cancer. Clin. Cancer Res. 23 (7), 1684–1689. https://doi.org/10.1158/1078-0432.CCR-16-0547.
Roelofs, A.J., et al., 2006. Molecular mechanisms of action of bisphosphonates: current status. Clin. Cancer Res. https://doi.org/10.1158/1078-0432.CCR-06-0843.
Salmaninejad, A., et al., 2019. Tumor-associated macrophages: role in cancer development and therapeutic implications. Cell. Oncol. https://doi.org/10.1007/s13402-019-00453-z.
Schindelin, J., et al., 2012. Fiji: an open-source platform for biological-image analysis. Nat. Methods 9 (7), 676–682. https://doi.org/10.1038/nmeth.2019.
Seider, M.J., et al., 2018. Randomized phase III trial to evaluate radiopharmaceuticals and zoledronic acid in the palliation of osteoblastic metastases from lung, breast, and prostate cancer: report of the NRG Oncology RTOG 0517 trial. Ann. Nucl. Med. 32 (8) https://doi.org/10.1007/s12149-018-1278-4.
Sethunath, V., et al., 2019. Targeting the mevalonate pathway to overcome acquired anti-HER2 treatment resistance in breast cancer. Mol. Cancer Res. 17 (11) https://doi.org/10.1158/1541-7786.MCR-19-0756.
Shmeeda, H., et al., 2013. Liposome encapsulation of zoledronic acid results in major changes in tissue distribution and increase in toxicity. J. Control. Release 167 (3). https://doi.org/10.1016/j.jconrel.2013.02.003.
Sousa, S., et al., 2015. Liposome encapsulated zoledronate favours M1-like behaviour in murine macrophages cultured with soluble factors from breast cancer cells. BMC Cancer 15 (1). https://doi.org/10.1186/s12885-015-1005-7.
Strobl, S., et al., 2018. Adjuvant bisphosphonate therapy in postmenopausal breast cancer. Curr. Treat. Options Oncol. 19 (4) https://doi.org/10.1007/s11864-018-0535-z.
Sun, C., et al., 2018. Tumor angiogenesis and bone metastasis - correlation in invasive breast carcinoma. J. Immunol. Methods 452. https://doi.org/10.1016/j.jim.2017.10.006.
Tanaka, Y., et al., 2017. Anti-tumor activity and immunotherapeutic potential of a bisphosphonate prodrug. Sci. Rep. 7 (1) https://doi.org/10.1038/s41598-017-05553-0.
Tanaka, Y., et al., 2018. Expansion of human γδ T cells for adoptive immunotherapy using a bisphosphonate prodrug. Cancer Sci. 109 (3) https://doi.org/10.1111/cas.13491.
van 't Hof, R.J., et al., 2017. Open source software for semi-automated histomorphometry of bone resorption and formation parameters. Bone 99. https://doi.org/10.1016/j.bone.2017.03.051.
Zhu, W., et al., 2019. Zoledronic acid promotes TLR-4-mediated M1 macrophage polarization in bisphosphonate-related osteonecrosis of the jaw. FASEB J. 33 (4) https://doi.org/10.1096/fj.201801791RR.
Zlatev, H.P., et al., 2016. Uptake of free, calcium-bound and liposomal encapsulated nitrogen containing bisphosphonates by breast cancer cells. Eur. J. Pharm. Sci. 86 https://doi.org/10.1016/j.ejps.2016.02.016.